International Journal of Modern Manufacturing Technologies
ISSN 2067–3604, Vol. XIV, No. 2 / 2022
https://doi.org/ 10.54684/ijmmt.2022.14.2.309

EFFECT OF TIG REMELTING ON PROPERTIES AND STRUCTURE OF WELDED JOINTS OF AUSTENITIC STAINLESS STEEL

Cyprian Tyszko[1], Jacek Górka [2]

[1]West Pomeranian University of Technology in Szczecin, POLITEST Materials Structure and Mechanical Properties Laboratory, al. Piastów 17, 70-310 Szczecin, Poland
[2] University of Technology, Mechanical Engineering Faculty, The Chair of Welding, Konarskiego 18a, 44-100 Gliwice, Poland

Corresponding author: Jacek Górka, jacek.gorka@polsl.pl

Abstract: One of the most commonly used corrosion resistant construction materials are austenitic stainless steels, mainly AISI 304. Any deviation from the welding technology in the case of this steel may result in welding defects or even loss of corrosion resistance. The purpose of this work was explored the influence of remelting using the TIG method (141) on the properties and structure of welded joints of AISI 304. The scope of this paper included making test joints of 2 mm thick sheets and then remelting them. The further part of this work consisted in carrying out: mechanical, macroscopic and microscopic examinations, hardness and corrosion resistance tests, SEM/EDS analysis. As a result of tests it was found that remelting of a joint causes a significant increase in hardness, lower elongation and general corrosion resistance, but increases the resistance to intercrystalline corrosion. Flexural strength and tensile strength were not changed by remelting.
Key words: TIG welding, austenitic stainless steel, remelting, interpass temperature, heat input.

1.INTRODUCTION

Construction materials with high corrosion resistance are frequently used in various industries. Due to their strength and physical properties they are used e.g. in automotive, food and petrochemical industries. On the other hand, for visual and aesthetic reasons, they can be found increasingly in the architecture and construction industry. Good corrosion resistance is unfortunately associated with the fact that engineers have been struggling with the difficulty of joining these materials for decades. Nowadays, the role of welding engineers is to develop such welding or mechanical joining process, so that construction of corrosion-resistant materials meet not only economic but also technological requirements. Among the most commonly used corrosion-resistant construction materials are certainly stainless steels. According to analysts at Grand View Research [1-3] the international stainless steel market was valued at $111.4 billion, while the forecast for 2027 predicts an increase in this value to $182.1 billion. The anticipated increase in the market value proves that year by year will increase also a demand for stainless steel products, both manufactured for the needs of heavy industry and consumer goods. According to the same report, 47.9% of the total stainless steel market in 2019 had the 300 series steels of the AISI/SAE standard, so it can be assumed that the most commonly used corrosion resistant steels are and will continue to be in the future austenitic steels [4-8]. Due to the wide range of applications, austenitic stainless steels can be joined by welding and brazing methods or mechanical methods e.g. by riveting or tightening screws. When tightness, high strength and inseparability are required, the only way to make the connection is using welding methods. Making a correct welding joint of austenitic steel requires not only the necessary knowledge, but also to observe the important rules before, during and after welding. Any deviation from the welding technology in the case of this steel may result in defects and welding inconsistencies or even loss of corrosion resistance. In smaller companies, whose production is not based on the EN 1090-2 standard, a frequent cause of defects and inconsistencies is welding of joints by personnel with low skills or without qualifications to weld a given type of joint. On the other hand, the cause may be intentional non-compliance of welders with the technological recommendations in company [9-11]. This reason, combined with not infrequently incomplete inspection of the finished product, gives the welders the opportunity to make arbitrary changes to the welding process. These factors, combined with the propensity of AISI 304 steel to form δ intermetallic phase, high susceptibility to hot cracking and the formation of Nb, Cr and Ti carbides, cause any additional amount of heat introduced to welding joint (e.g. during remelting to correct joint

asymmetry or lack of remelting) can affect the properties and structure of the resulting joint [12-16]. While in the case of responsible construction, the welding procedures must be qualified in accordance with the provisions of the EN 1090-2 standard and the entire welding process must be supervised, in the case of products that do not require regulatory approval or acceptance, there is a risk that due to remelting the customer will receive defective product [17-21].

2. MATERIALS AND METHOD

The purpose of this work was explored the influence of remelting by using the TIG method (141) on the properties and structure of welded joints of austenitic stainless steel AISI 304. To check this, test joints of 2 mm thick sheets were made and then they were remelted using the TIG method (141) in two different ways: with the interpass temperature maintenance and immediately after welding. The AISI 304 sheet was characterized by a surface finish 2B, meaning that it was cold rolled, annealed and pickled, as well as additionally temper rolled. The chemical composition and mechanical properties of the steel used are shown in Tables 1 and 2, while the structure is shown in Figure 1.

Table 1. Chemical composition of AISI 304 steel [% Wt.]

C	Si	Mn	P	S	Cr	Ni
0.05	0.42	1.35	0.035	0.014	18.2	8.75

Table 2. Mechanical properties of AISI 304 steel used

$R_{0,2}$ [N/mm^2]	R_m [N/mm^2]	A [%]
≥230	540-750	≥45

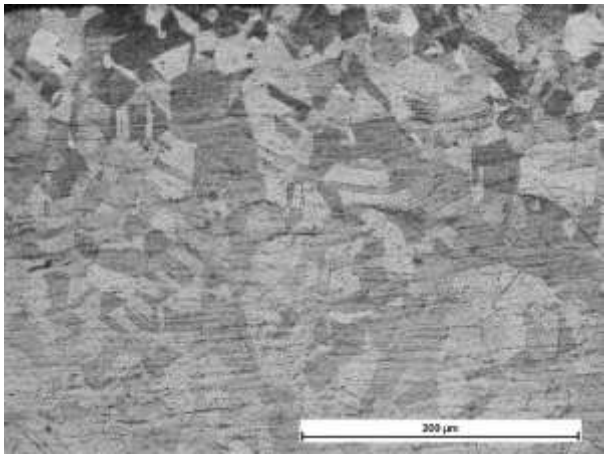

Fig. 1. Microstructure of the tested steel AISI 304, pickling: electrolytic in HNO_3 - distilled water solution.

As filler material was used solid rod of 2 mm diameter Lincoln Electric LNT 304L. The chemical composition and mechanical properties of the filler material alloy are shown in Tables 3 and 4.

Table 3. Chemical composition of filler material Lincoln Electric LNT 304L

C [%wt.]	Si [%wt.]	Mn [%wt.]	Cr [%wt.]	Ni [%wt.]	Mo [%wt.]
0.01	0.4	1.7	20	10	0.1

Table 4. Mechanical properties of filler material Lincoln Electric LNT 304L

$R_{0,2}$ [N/mm^2]	R_m [N/mm^2]	A [%]	KV +20℃ [J]	KV -196℃[J]
472	692	34	120	91

As a shielding and forming gas was used group I1 gas according to EN ISO 14175, specifically compressed argon gas produced by Air Liquide company with the trade name ALPHAGAZ 1 Ar. The specification of the gas used is shown in Table 5.

Table 5. Specification of shielding and forming gas Air Liquide ALPHAGAZ 1 Ar

Purity [%]	H_20 [ppm]	O_2 [ppm]	C_nH_m [ppm]
99.999	≤ 3	≤ 2	≤ 0.5

The test joints were made by the TIG method using Castolin Eutectic CastoTIG 2002 AC/DC welding device. The joints were made also with the use of WT20 electrodes with a diameter of 2.4 mm, designed for welding high-alloyed steels with direct current with negative polarity. Before welding, the edges of the joined parts were milled to even out the surface and remove areas thermally threated during the cutting process. Because of the necessity for root covering during welding of austenitic stainless steel, joints were made on a copper pad with channels supplying the forming gas. Tack welds were made every 125 mm. The type of bevelling and the distance between welded elements were selected on the basis of the EN ISO 9692-1 standard, according to which butt joints of 2 mm thick sheets should be welded one-sided. In accordance with the recommendations of this standard, the test joints were made as a square groove weld with 2 mm opening. In order to identify specific test joints, designations were introduced and are shown in Table 6.

Table 6. Test joints designations

Test joint designations	Method of welding
I	Single-welded joint with filler material
II	Single-welded joint with filler material, remelted with maintaining the interpass temperature of 150℃
III	Single-welded joint with filler material, remelted without maintaining the interpass temperature of 150℃

The same parameters were used for the making of the welded joints and the subsequent remelting. The only

difference was the filler material which was added for making the welds, while remelting was carried out using only the material from the previous joint. The welding and remelting process parameters are shown in Table 7.

Table 7. Welding and remelting process parameters

Current [A]	Voltage [V]	Welding speed [mm/s]	Shield gas rate [l/min]	Forming gas rate [l/min]	Polarity	Gas nozzle size	Welding position	Heat input [kJ/mm]
75	13	3	11	6	DC-	6	PA	0.234

2.1 Macroscopic examinations

For macroscopic examinations, 20x30 mm test samples were cut from each joint and then clad, sanded and polished. The samples were subsequently electrolytically etched in a solution of HNO3 - distilled water in the proportions of 6:4. The macrostructure was observed using an Olympus SZX9 microscope with an installed PC camera Moticam 5+.

2.2 Microscopic examinations

For the microscopic examinations were used exactly the same samples as for the macroscopic examinations. Images of weld and SWC were taken on unchanged samples, i.e. electrolytically etched in accordance with subsection 3.1. After these images were taken, in order to make the structure of the parent metal more clearly visible, the samples were etched again in HCl - HNO_3 solution in the proportion of 3:1. The echting time was 3 seconds. On such prepared samples using a Nikon Eclipse MA100 microscope, were taken microscopic images with 200x magnification.

2.3 Hardness tests

Hardness was measured using a Wilson Wolpert Micro-Vickers 401 MVD hardness tester with an indenter force of 4.903 N and an indenter time of 10 seconds. The contact force and indenter parameters determined the interpretation of the test results as hardness on the Vickers HV0.5 scale. The starting point of the measurements was the intersection of the two axes of the weld-section and were taken 15 measurements in each direction along the horizontal axis of the section (one measurement every 0.2 mm).

2.4 Mechanical examinations

For the bending test, were cut two 20x250 mm samples from each of the test joints (one for cap and and one for roof tension). The test was carried out and evaluated based on EN ISO 5173 standard. The samples were placed in a hydraulic press equipped with a bending pin with a diameter of 12 mm and two supports with a spacing of 25 mm. The samples were deformed by applying a load at the weld area and bent to 135°. For the static tensile test, were cut three samples from each of the test joints. The tensile test was carried out on a computer-controlled testing machine equipped with extensometers. The test was performed in accordance with the assumptions of EN ISO 6892-1 standard.

2.5 Corrosion resistance tests

For the NSS corrosion resistance test (general corrosion test), were cut samples of approximately 75x85 mm from each of the test joints. All the samples were weighed with an accuracy of 0.0001 g and were measured the dimensions needed to calculate their surface area. NSS corrosion resistance tests were carried out in accordance with ISO 9227 standard. The samples were placed in the Ascott CC450iP salt chamber for the time required by the above mentioned standard, i.e. 168 hours. The test consisted of exposing the samples in a mist atmosphere formed by mixing 5% NaCl solution with air at 35°C. After 168 hours, the samples were removed from the salt chamber, weighed and their dimensions were measured once again. On the basis of the obtained measurements, were calculated the weight loss and the linear corrosion rate. Before the Huey test (intercrystalline corrosion test), simiralry to the NSS test, each sample was weighed to an accuracy of 0.0001 g and were measured the dimensions needed to calculate its surface area. The test consisted of immersing the samples in concentrated HNO_3 and then bringing it to a boil and maintaining this process for 48 hours. After this time, the samples were removed, weighed and their dimensions were measured once again. On the basis of the obtained measurements, were calculated the weight loss and the linear corrosion rate.

2.6 SEM/EDS analysis

For the base material and each joint was carried out SEM/EDS analysis, which made it possible to determine the elemental composition of the individual structural components and to confirm the presence of precipitates.

3. RESULTS AND DISCUSSION

3.1 Macroscopic examinations

Macroscopic pictures of test joints taken at 12,5x magnification are shown in Figure 2-4.

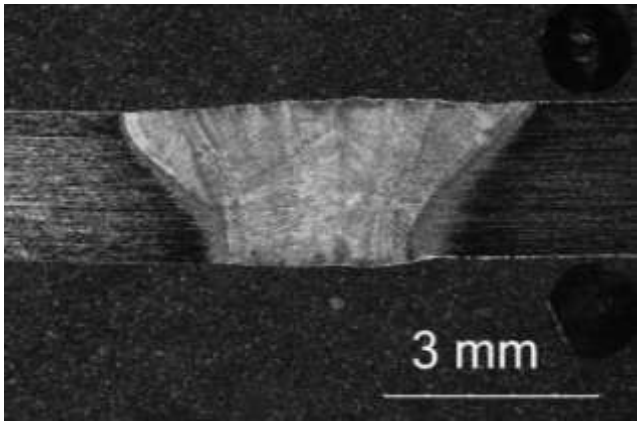

Fig. 2. Macrostructure of a single-welded joint with filler material – test joint I, etching: electrolytic in HNO_3 - distilled water solution.

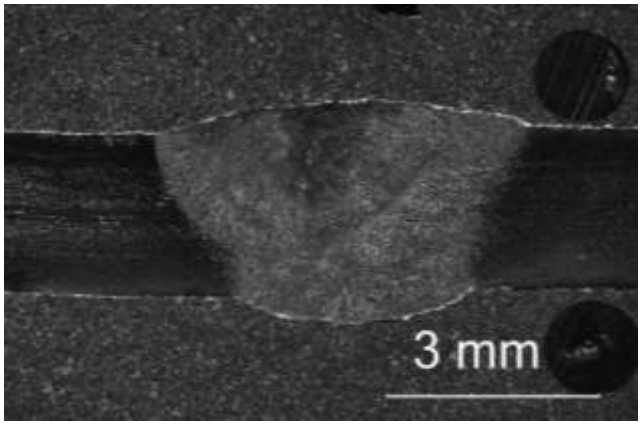

Fig. 3. Macrostructure of a single-welded joint with filler material, remelted with maintaining the interpass temperature of 150℃– test joint II, etching: electrolytic in HNO_3 - distilled water solution.

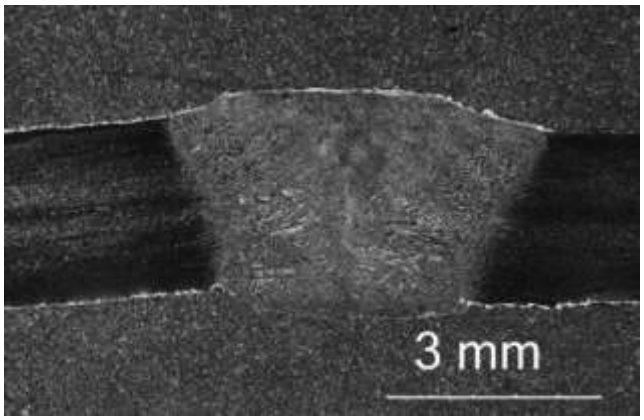

Fig. 4. Macrostructure of a single-welded joint with filler material, remelted without maintaining the interpass temperature of 150℃– test joint III, etching: electrolytic in HNO_3 - distilled water solution.

The macroscopic examination showed that none of the test joints contained internal weld inconsistencies. Only in the case of the unmelted joint (I) were a clear fusion line and a heat affected zone visible. A dendritic structure was found in each of the samples, which was the result of uneven heat dissipation during the solidification process. In the joint melted without maintaining the interpass temperature (III), its presence was apparently noticeable. The pronounced asymmetry between the left and right sides of each test weld and the HAZ is the result of uneven heating of the elements during welding and is caused by the irregular setting of the TIG torch.

3.2 Microscopic examinations

Microscopic images of the parent metal, HAZ and weld are shown in Figure 5-11.

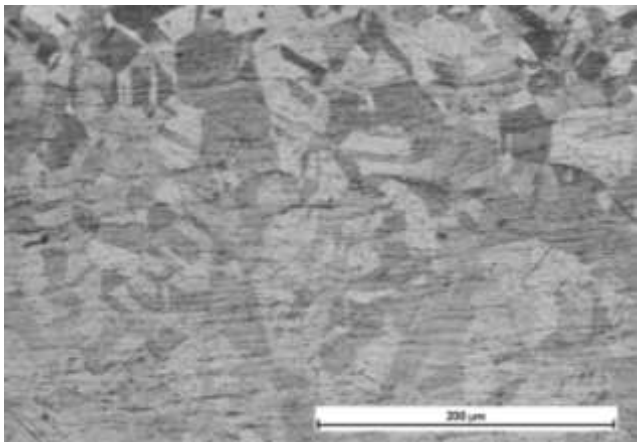
Fig. 5. Microstructure of the parent metal in the tested joints, etching: electrolytic in HCl - HNO_3 solution.

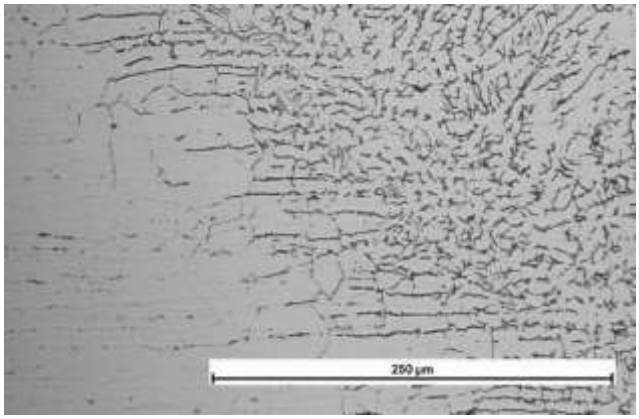

Fig. 6. Microstructure of the HAZ and weld in the tested joint I, etching: electrolytic in HCl - HNO_3 solution.

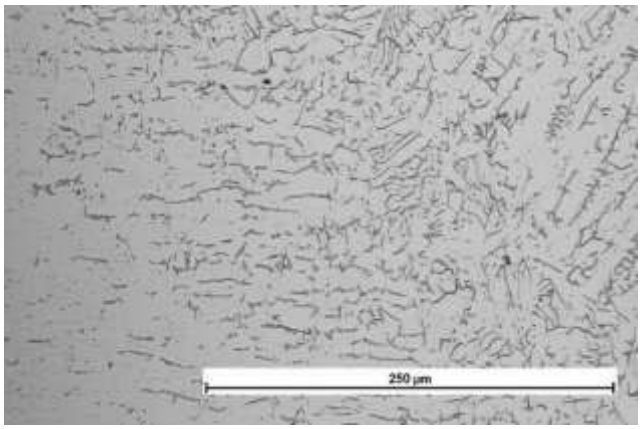

Fig. 7. Microstructure of the HAZ and weld in the tested joint II, etching: electrolytic in HCl - HNO_3 solution.

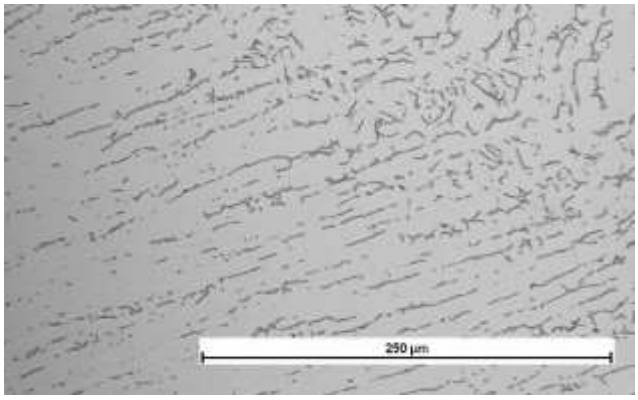

Fig. 8. Microstructure of the HAZ and weld in the tested joint III, etching: electrolytic in HCl - HNO_3 solution.

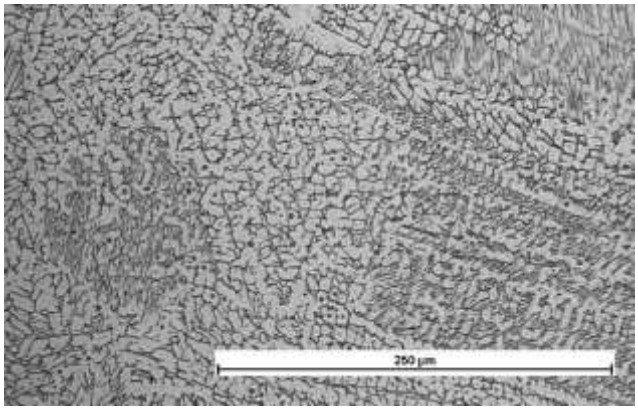

Fig. 9. Microstructure of the weld in the tested joint I, etching: electrolytic in HCl - HNO_3 solution.

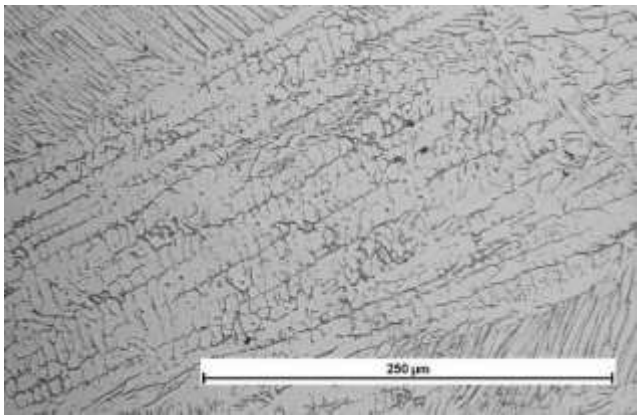

Fig. 10. Microstructure of the weld in the tested joint II, etching: electrolytic in HCl - HNO_3 solution.

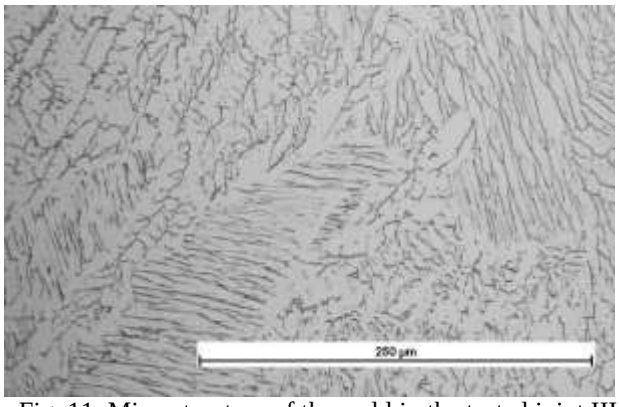

Fig. 11. Microstructure of the weld in the tested joint III, etching: electrolytic in HCl - HNO_3 solution

Microscopic examination of the parent material revealed the presence of annealing twins and banded δ-ferrite, which are the result of cold rolling and segregation of ferritizers. In the case of each of the test joints, the heat affected zone had an austenitic structure with skeletal δ-ferrite and interdendritic ferrite. It was also found that in the case of the HAZ of a non-melted joint (I) the austenite grain size was the smallest, whereas it was the largest in the remelted joint without maintaining the interpass temperature of 150℃ (III). In joint non-melted (I) and joint remelted with maintaining the interpass temperature (II) the parent material and the HAZ were observed separations of chromium carbides $Cr_{23}C_6$ and σ-phase on the austenite-ferrite interfaces, while in the joint remelted without maintaining the interpass temperature (III) this separations have dissolved. The weld in each of the test joints had an austenitic structure with skeletal and lathy δ-ferrite forms. In the non-melted joint (I), in the skeletal ferrite areas, separations of the σ-phase were clearly visible and in the whole weld area were distributed chromium carbides $Cr_{23}C_6$. In the weld remelted with maintaining the interpass temperature (II), trace amounts of precipitates were revealed, whereas in the weld which was remelted immediately after welding (III) the precipitates were almost completely dissolved. Along with the decrease in the amount of precipitates after the remelting process was observed a significant increase of the austenite grain size, especially in the joint without maintaining the interpass temperature of 150℃ (III).

3.3 Hardness tests

A comparison of the average hardness of individual test joints is shown in Figure 12.

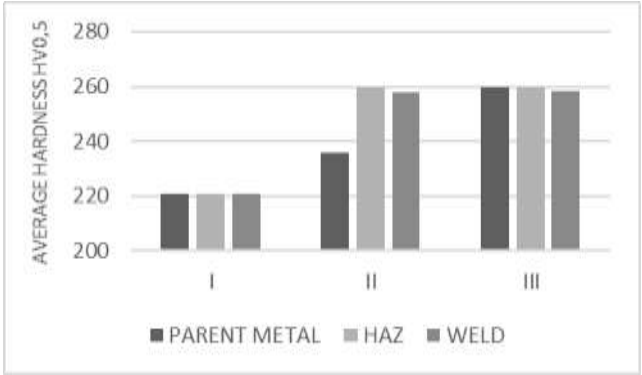

Fig. 12. Comparison of the average hardness of individual test joints (with division into weld zones).

As a result of tests of hardness using the Vickers HV0.5 method, it was found that the hardness of the test joint not subjected to remelting (I), in each zone is within the values declared by major manufacturers for steel AISI 304. In the case of remelted joints, each zone hardened in comparision to the parent metal, but

the hardness in the remelted joint without maintaining the interpass temperature (III), the hardness increased the most (it was about 30 HV0.5 more than the maximum declared values for the tested steel).

3.4 Mechanical examinations

Samples after the bending test are shown in Figure 13-15.

Fig. 13. Samples of joint I after bending test.

Fig. 14. Samples of joint II after bending test.

Fig. 15. Samples of joint III after bending test.

Bending tests from the cap and the roof sides to a bending angle of 135° did show any damage to the joints. In the sample of a non-melted joint (I) bend occurred in the weld area, whereas in the remelted joint samples (II,III) outside the welding joint. This test confirmed an increase in the hardness of the weld area in both joints in comparision to the parent metal.

Samples after the static tensile test are shown in Figure 16-18 and tensile test graphs (stress – strain curves) are shown in Figure 19-21.

Fig. 16. Samples of joint I after static tensile test.

Fig. 17. Samples of joint II after static tensile test.

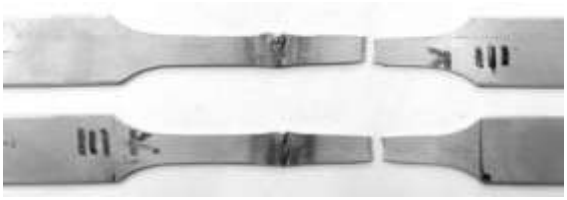

Fig. 18. Samples of joint III after static tensile test.

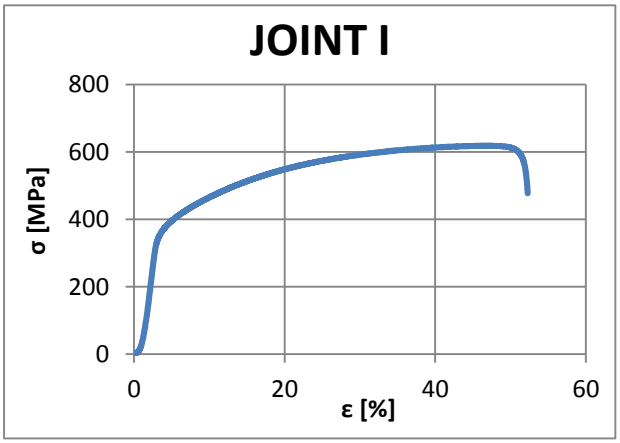

Fig. 19. Stress - strain curve for joint I.

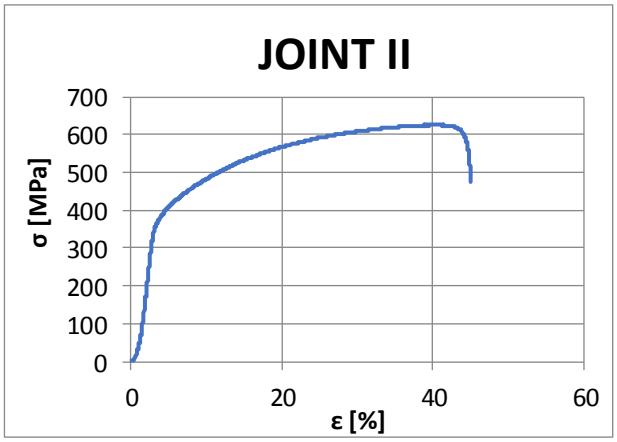

Fig. 20. Stress - strain curve for joint II.

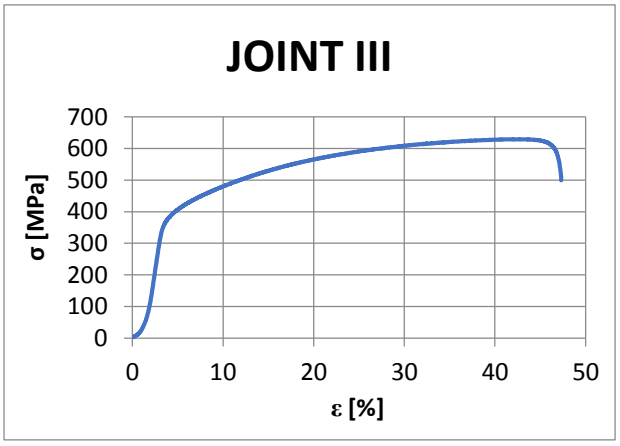

Fig. 21. Stress - strain curve for joint III.

The carried out static tensile test showed that the tensile strength of all the samples was within the range 625-628 MPa, which indicates a negligible

effect of remelting on this parameter. The breaking of each sample occurred in the region of the native material. The remelting noticeably worsened the elongation of the samples, but the elongation values for each of the joints were within the range defined in EN 10088-2 standard [12]. Results of mechanical examinations are shown in Table 8.

Table 8. Results of mechanical examinations

Test joint	Tensile strenght [MPa]	Elongation [%]	Bending angle [°]	Bending note
I	626	52.5	135	positive
II	625	46	135	positive
III	628	47.5	135	positive

3.5 Corrosion resistance tests

Comparison of the corrosion test results are shown in Table 9.

Table 9. Comparison of the corrosion test results

Test joint	NSS test		Huey test	
	Weight loss [g/m^{2}day]	Linear corrosion rate [mm/year]	Weight loss [g/m^{2}day]	Linear corrosion rate [mm/year]
I	0.01653	7.63 x 10^{-5}	17.1519	0.0792
II	0.02874	1.32 x 10^{-4}	3.8310	0.0177
III	0.03184	1.47 x 10^{-4}	16.1322	0.0742

The NSS corrosion resistance test showed that in the case of a joint remelted with maintaining the interpass temperature (II) the linear corrosion rate is the highest, while for a non-melted joint (I) is the lowest. This is a result from the higher oxidation state of the remelted joint surface in comparison to the single-welded joint. On the basis of the Huey test, it was estimated that the remelted joint with maintaining the interpass temperature (II) has the best corrosion resistance, which is probably due to the reduced carbide content compared to the non-melted joint (I) and lower segregation of alloying elements in relation to the joint remelted immediately after welding (III).

3.6 SEM/EDS analysis

SEM image of the parent metal taken at 2000x magnification is shown in Figure 22. SEM images of the HAZ of non-melted joint (I) are shown in Figure 23 and 24. SEM image of the weld of single-welded non-melted joint (I) is shown in Figure 25. Table 10 includes elemental composition point 1 and 2, marked on the Figure 23-25.

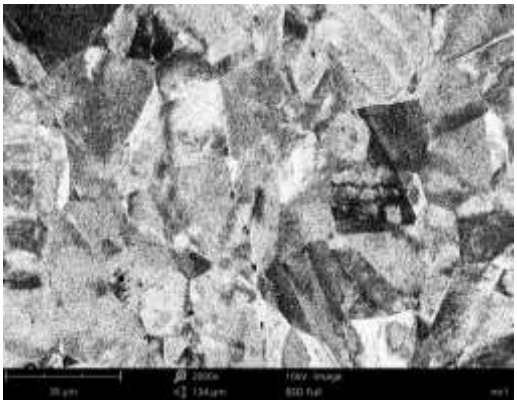

Fig. 22. SEM image of microstructure of the parent metal.

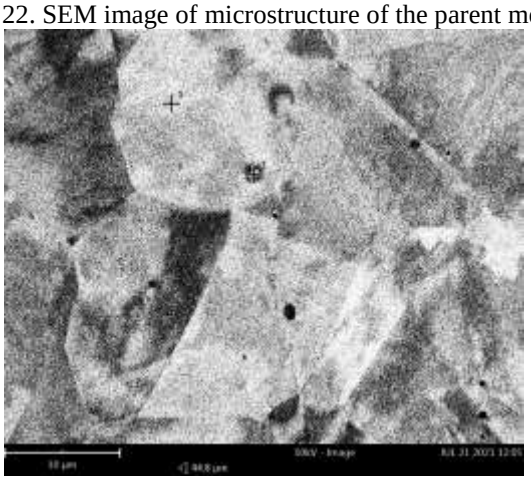

Fig. 23. SEM image of microstructure of the HAZ of single-welded non-melted joint (I).

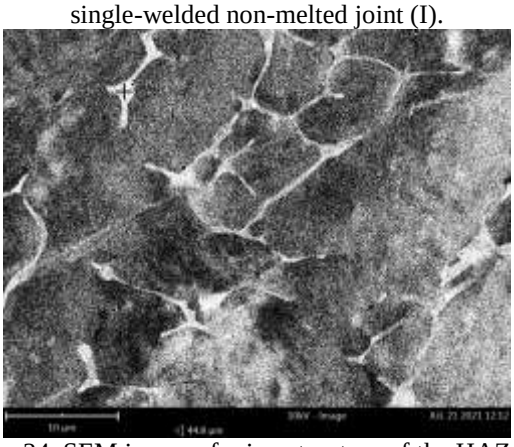

Fig. 24. SEM image of microstructure of the HAZ of single-welded non-melted joint (I).

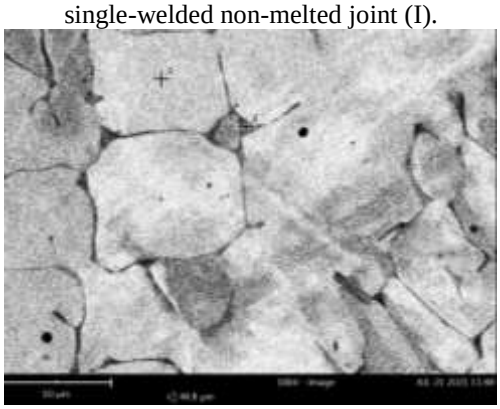

Fig. 25. SEM image of microstructure of the weld of single-welded non-melted joint (I).

Table 10. EDM analysis of single-welded non-melted joint (I) results taken from Figure 23-25

Point	Fe [% Wt.]	Cr [% Wt.]	Ni [% Wt.]	C [% Wt.]
1 (Figure 23)	75.18	16.82	7.99	-
2 (Figure 23)	71.13	18.23	10.64	-
1 (Figure 24)	73.88	17.50	8.61	-
2 (Figure 24)	70.69	21.56	-	7.21
1 (Figure 25)	70.46	18.66	10.88	-
2 (Figure 25)	72.34	23.82	3.84	-

Based on a Figure 22, it was determined that the parent material had a fully austenitic structure. The HAZ of single-welded non-melted joint (I), which was shown in Figure 23 and 24, had an austenitic structure with point-like precipitates of chromium carbides at the austenite-ferrite boundaries (Point 2 – Figure 24) and presence of high-temperature δ-ferrite (Point 2 – Figure 23). The weld of single-welded non-melted joint (Figure 25) had a structure similar to the HAZ, except that additionally it was observed the occurrence of a σ-phase characterized by a high chromium and a low nickel content (Point 2 – Figure 25).

SEM image of the HAZ of single-welded joint remelted with maintaining the interpass temperature of 150℃ (II) is shown in Figure 26. The weld of single-welded joint remelted with maintaining the interpass temperature of 150℃ (II) is shown in Figure 27. Table 11 includes elemental composition point 1,2 and 3, marked on the Figure 26 and 27.

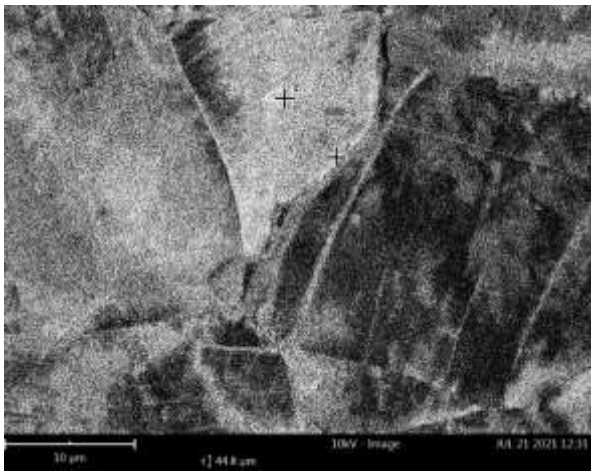

Fig. 26. SEM image of microstructure of the HAZ of single-welded joint remelted with maintaining the interpass temperature of 150℃ (II).

The HAZ of single-welded joint remelted with maintaining the interpass temperature of 150℃ (II), which was shown in Figure 26, had an austenitic structure with a slight presence of high-temperature δ-ferrite. The weld of single-welded joint remelted with maintaining the interpass temperature of 150℃ (Figure 27) had whereas an austenitic structure (Point 1 – Figure 27) with separations of chromium carbides (Point 3 – Figure 27), σ-phase (Point 2 – Figure 27) and δ-ferrite. The precipitates in this joint were far less noticeable than in the test joint I.

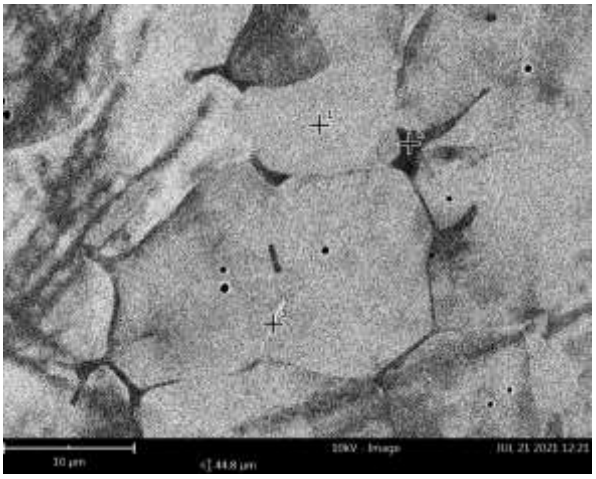

Fig. 27. SEM image of microstructure of the weld of single-welded joint remelted with maintaining the interpass temperature of 150℃ (II).

Table 11. EDM analysis of single-welded joint remelted with maintaining the interpass temperature of 150℃ (II) results taken from Figure 26 and 27

Point	Fe [% Wt.]	Cr [% Wt.]	Ni [% Wt.]	C [% Wt.]
1 (Figure 26)	71.43	17.45	11.13	-
2 (Figure 26)	71.45	18.27	10.29	-
1 (Figure 27)	69.84	18.99	11.18	-
2 (Figure 27)	68.97	22.68	8.34	-
3 (Figure 27)	64.65	22.30	2.00	22.30

SEM image of the HAZ of single-welded joint remelted without maintaining the interpass temperature of 150℃ (III) is shown in Figure 28. SEM image of the weld of single-welded joint remelted without maintaining the interpass temperature of 150℃ (III) is shown in Figure 29. Table 12 includes elemental composition point 1-4, marked on the Figure 28 and 29.

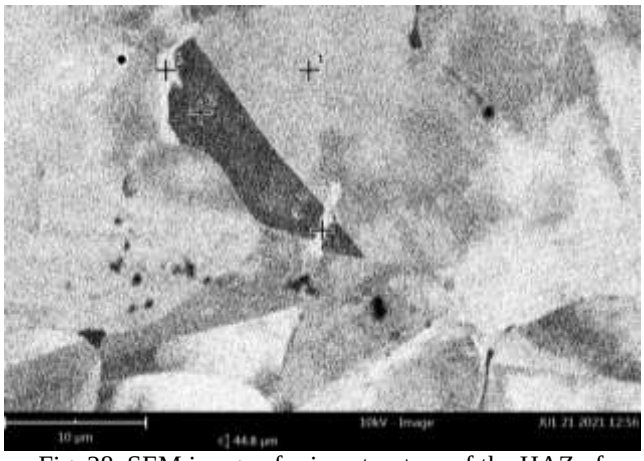

Fig. 28. SEM image of microstructure of the HAZ of single-welded joint remelted without maintaining the interpass temperature of 150℃ (III).

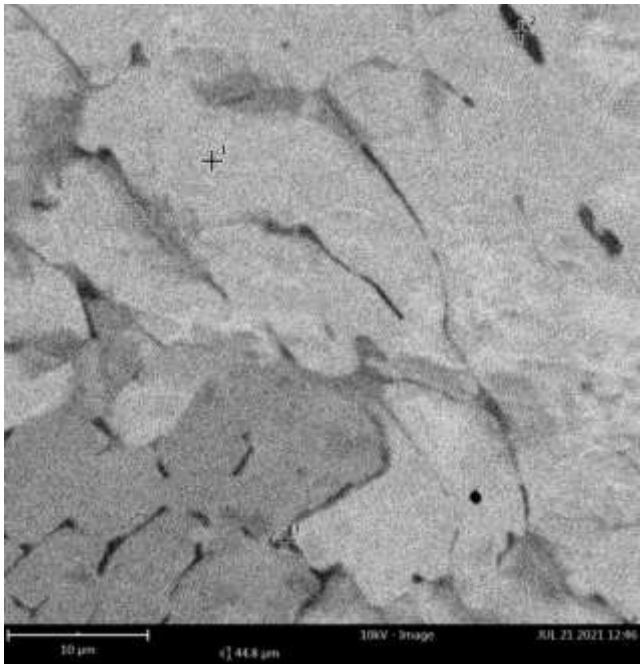

Fig. 29. SEM image of microstructure of the weld of single-welded joint remelted without maintaining the interpass temperature of 150℃ (III).

Table 12. EDM analysis of single-welded joint remelted with maintaining the interpass temperature of 150℃ (II) results taken from Figure 17 and 18

Point	Fe [% Wt.]	Cr [% Wt.]	Ni [% Wt.]	C [% Wt.]
1 (Figure 28)	72.01	16.51	11.48	-
2 (Figure 28)	73.59	15.13	11.28	-
3 (Figure 28)	59.61	23.78	6.35	10.26
4 (Figure 28)	62.86	18.95	5.66	11.27
1 (Figure 29)	71.00	17.02	11.98	-
2 (Figure 29)	73.37	24.20	2.43	-
3 (Figure 29)	70.71	23.64	5.65	-

The HAZ of single-welded joint remelted without maintaining the interpass temperature of 150℃ (III), which was shown in Figure 28, had an austenitic structure (Point 1 – Figure 28) with precipitates of high-temperature δ-ferrite and chromium carbides (Point 3 and 4 – Figure 28). The weld of single-welded joint remelted without maintaining the interpass temperature of 150℃ (Figure 29) had whereas an austenitic structure (Point 1 – Figure 29) with separations of σ-phase (Point 2 and 3 – Figure 29) and δ-ferrite.

4. CONCLUSIONS

For joining thin austenitic stainless steel sheets, remelting causes a deterioration of joint properties. Despite the resistance to intercrystalline corrosion is improved due to dissolution of σ-phase precipitates and chromium carbides, but as a result of strong oxidation of the joint surface and austenite grain growth, its resistance to general corrosion deteriorates and elongation decreases. In addition, the hardness of the joint increases to the maximum values above declared by manufacturers for the parent metal. On the basis of the microstructure and hardness testing it can be assumed that the remelted joint will also be characterised by a lower impact strength, however, this could not be verified due to the thinness of the welded pieces. In order to produce a joint with the optimum combination of strength properties, ductility and corrosion resistance, remelting of joints should be avoided.

5. REFERENCES

1. Schino A., (2007) *Manufacturing and Application of Stainless Steels*, MPDI AG, Basel
2. Adamiak, M., Wyględacz, B., Czupryński, A., Górka, J. (2017). *A study of susceptibility and evaluation of causes of cracks formation in braze-weld filler metal in lap joints aluminum – carbon steel made with use of CMT method and high power diode laser*, Archives of Metallurgy and Materials, 62, 2113-2123
3. Ahmadi, E., Ebrahimi, A.R. (2013). *The effect of activating fluxes on 316L stainless steel weld joint characteristic in TIG welding using the Taguchi method*, Journal of Advanced and processing, 1(1), page: 55.
4. Folkhard E., (1984) *Welding Metallurgy of Stainless Steels*, Springer-Verlag, Wien
5. Lippold J., Kotecki D., (2005) *Welding metallurgy and weldability of stainless steels*, John Wiley & Sons Inc., New Jersey
6. Łabanowski J., (2019) *Stale odporne na korozję i ich spawalność*, Wydawnictwo Politechniki Gdańskiej, Gdańsk.
7. Tasak E., Ziewiec., (2009) *Spawalność materiałów konstrukcyjnych. Tom 1. Spawalność stali*, Wydawnictwo JAK, Kraków.
8. Gietka, T., Ciechacki, K., Kik, T. (2016). *Numerical simulation of duplex steel multipass welding*, Archives of Metallurgy and Materials, 61, 1975-1983.
9. Górka, J., Janicki, D., Fidali, M., Jamrozik, W. (2017). *Thermographic Assessment of the HAZ Properties and Structure of Thermomechanically Treated Steel*, International Journal of Thermophysics, 38, pp. 183.
10. Grand View Research: Stainless Steel Market Size, Share & Trends Analysis Report By Grade (200 Series, 300 Series, 400 Series, Duplex Series), By Product (Flat, Long), By Application (Building & Construction, Heavy Industry), By Region, And Segment Forecasts. Available from: https://www.grandviewresearch.com/industry-analysis/stainless-steel-market, Accessed: 13/06/2021
11. Górka, J., Przybyła, M,. Szmul, M., Chudzio, A., Ładak D. (2019). *Orbital TIG welding of titanium*

tubes with perforated bottom made of titanium-cald steel, Advances in Materials Science, 3(61), 55-64.
12. Gucwa, M., Winczek, J., Giza, K., et. Al. (2019). T*he Effect of Welding Methods on the Corrosion Resistance of 304 Stainless Steel Joints*, Acta Physica Polonica A, 135(2), 232-235.
13. Swierczynska, A., Labanowski, J., Michalska, J. et al., (2017*). Corrosion behavior of hydrogen charged super duplex stainless steel welded joints*, Materials and Corrosion-Werkstoffe und Korrosion, 68 (10), 1037-1045.
14. Kciuk, M., Lasok, S. (2017). *Corrosion resistance of X5CRNI18-10 stainless steel*, Archives of Metallurgy and Materials, 62(4), 2101-2106.
15. Skowronska, B., Chmielewski, T., Pachla, W., et. al. (2019). *Friction weldability of UFG 316L stainless steel*, Archives of Metallurgy and Materials, 64(3), 1051-1058.
16. Rogalski, G., Swierczyńska, A., Landowski, M., Fydrych, D. (2020). *Mechanical and Microstructural Characterization of TIG Welded Dissimilar Joints between 304L Austenitic Stainless Steel and Incoloy 800HT Nickel Alloy*, Metals, 10(5), 559.
17. Kik, T., Moravec, J., Novakova, I. (2017). *New method of processing heat treatment experiments with numerical simulation support*, IOP Conference Series-Materials Science and Engineering Volume: 227.
18. Kurc-Lisiecka, A., Ozgowicz, W.S., Kalinowska-Ozgowicz, E., Maziarz, W. (2016). *The microstructure of metastable austenite in X5CrNi18-10 steel after its strain-induced martensitic transformation*, Materials and Technologies, 50(6), 837-843.
19. Morawiński, Ł., Chmielewski, T., Olejnik, L., Buffa, G., Campanella, D., Fratini, L. (2018). *Welding abilities of UFG metals*, AIP Conference Proceedings 1960(1), ESAFORM, Palermo, Italy
20. Parkitny R., Winczek J., (2013). *Analytical solution of temporary temperature field in half-infinite body caused by moving tilted volumetric heat source*, International Journal of Heat and Mass Transfer, 60, 469 – 479.
21. Available from: https://www.lincolnelectric.com /assets/global/Products/ConsumableEU_TIGWires-LNT-LNT304L/LNT304L-ENG.pdf, Accessed: 13/06/2021

Received: May 18, 2022 / Accepted: December 15, 2022 / Paper available online: December 20, 2022 © International Journal of Modern Manufacturing Technologies